Influence of Rubber Particle Size on Mechanical Properties of Polypropylene–SEBS Blends

F. STRICKER, Y. THOMANN, R. MÜLHAUPT

Freiburger Materialforschungszentrum und Institut für Makromolekulare Chemie der Albert-Ludwigs-Universität, Stefan-Meier-Straße 21, D-79104 Freiburg i. Br., Germany

Received 3 September 1997; accepted 4 October 1997

ABSTRACT: Isotactic polypropylene blends with 0–20 vol % thermoplastic elastomers were prepared to study the influence of elastomer particle size on mechanical properties. Polystyrene-*block*-poly(ethene-*co*-but-1-ene)-*block*-polystyrene (SEBS) was used as thermoplastic elastomer. SEBS particle size, determined by means of transmission electron and atomic force microscopy, was varied by using polypropylene and SEBS of different molecular weight. With increasing polypropylene molecular weight and, consequently, melt viscosity and decreasing SEBS molecular weight, SEBS particle size decreases. Impact strength of pure polypropylene is almost independent of molecular weight, whereas impact strength of polypropylene blends increases strongly with increasing polypropylene molecular weight. The observed sharp brittle–tough transition is caused by micromechanical processes, mostly shear yielding, especially occurring below a critical interparticle distance. The interparticle distance is decreasing with decreasing SEBS particle size and increasing volume fraction. If the polypropylene matrix ligament between the SEBS particles is thinner than 0.27 μm, the blends become ductile. Stiffness and yield stress of polypropylene and polypropylene blends increase with increasing polypropylene molecular weight in the same extent, and are consequently only dependent on matrix properties and not on SEBS particle size. © 1998 John Wiley & Sons, Inc. J Appl Polym Sci 68: 1891–1901, 1998

Key words: polypropylene; blends; particle size; interparticle distance; impact strength

INTRODUCTION

Blends of isotactic polypropylene (*i*-PP) with various impact modifiers, such as ethylene–propylene copolymers, ethylene–propylene–diene, and butadiene–styrene–acrylonitrile terpolymers have been investigated extensively.[1,2] As a thermoplastic elastomer, the triblock copolymer polystyrene–*block*-poly(ethylene-*co*-but-1-ene)–*block*-polystyrene (SEBS), which can be obtained by hydrogenation of the butadiene sequence of the corresponding polystyrene–*block*-polybutadiene–*block*-polystyrene triblock copolymer,[3] is of growing interest. This is due to higher service temperature and solvent resistance of such blends with respect to those containing diene-based rubbers.[4] Gupta and Purwar investigated mechanical, dynamic–mechanical, and rheological properties of *i*-PP blends as a function of SEBS content, as well as crystallization behavior.[5–8] A sharp brittle–tough transition was observed at SEBS contents of about 15 vol %. Wu and a coworker interpretated a similar transition of nylon–rubber blends with the percolation model for rubber toughening.[9–11] Below a critical matrix ligament thickness that can be calculated from elastomer particle size and volume fraction, blends show ductile behavior. The origin of this effect is not fully understood because it is likely that several

Correspondence to: R. Mülhaupt.
Contract grant sponsor: Shell Research.

Journal of Applied Polymer Science, Vol. 68, 1891–1901 (1998)
 CCC 0021-8995/98/121891-11

mechanisms contribute to the brittle–tough transition. Only when the matrix ligament is thinner than a critical value, stress concentrations around the elastomer particles can overlap, making local shear yielding easier. Another effective mechanism for enhanced toughness is the cavitation of the elastomer particles. Borggreve et al. explained the critical particle distance with a transition from plane strain to plain stress conditions.[12,13] Plain stress conditions allow shear yielding, and the blends are tough. When the matrix ligament is thicker than the critical value, such a transition does not occur, and the matrix ligament fails in a brittle fashion. Wu determined for nylon–rubber blends a critical matrix ligament thickness of 0.3 μm,[10,11] and Van der Sanden et al. found for polystyrene blends a critical value of 0.05 μm.[14]

The present article describes the influence of molecular weight of the blend components on the morphology of *i*-PP–SEBS blends and the consequences on the mechanical properties of the blends, especially impact strength. Four isotactic polypropenes (*i*-PP) and two polystyrene–*block*-poly(ethene-*co*-but-1-ene)–*block*-polystyrene (SEBS) thermoplastic elastomers with different molecular weight were blended in a twin-screw extruder at 300 rpm and a maximum processing temperature of 230°C. The SEBS particle size was determined by means of transmission electron microscopy (TEM) and correlated with the matrix ligament thickness in order to determine the critical interparticle distance for brittle–tough transition of *i*-PP blends.

EXPERIMENTAL

Materials

All polymers were commercial grades, supplied by Shell (Ottignies-Louvain-La-Neuve, Belgium), and used without further purification. Four isotactic polypropylenes and two polystyrene–*block*-poly(ethene-*co*-but-1-ene)–*block*-polystyrenes (Kraton G, abbreviated SEBS) with different molecular weights were used in this study. Table I summarizes molecular weights, tacticities, and structural data of all polymers used in this study.

Blend Preparation

All blends were prepared using identical mixing and molding conditions. SEBS volume fraction was varied between 0 and 20 vol %. Melt blending was performed in a twin-screw extruder (ZSK25, Werner & Pfleiderer) with 300 rpm and a maximum temperature of 230°C. 0.2 wt % Irganox1010/Irgafos 168 (4/1 wt %) were added as stabilizers during melt processing. The extruded materials were injection-molded to obtain specimen for mechanical testings and morphological studies.

Mechanical Properties

Tensile properties were measured on an Instron (Model 4202) tensile machine according to ISO 527 standard procedure, using a crosshead speed of 1 mm/min for determination of the Young's modulus and 50 mm/min for yield stress and elongation to break. Izod impact strength was determined on notched samples according to ISO 180/1A using test specimen of 60 × 10 × 4 mm. The average deviations of Young's modulus and impact strength were approximately 3%; of yield stress, 1%; and of elongation to break, 15%. At least 5 samples were tested for each blend, and the average value was reported. Tests were performed at ambient temperature (23 ± 2°C).

Transmission Electron Microscopy

TEM measurements for particle size determination were performed using a Zeiss CEM 902 transmission electron microscope, applying an acceleration voltage of 80 kV. The specimen were cut at room temperature perpendicular to the flow direction of the injection molding process by an ultramicrotome (Ultracut E, Reichert & Jung, equipped with a diamond knife). Ultrathin sections of approximately 100 nm thickness were stained with RuO_4 prepared from 10 mg $RuCl_3$ and 0.5 mL of 10 wt % NaClO solution.[15] After 5 min in RuO_4 gas phase, only the PS domains of the block copolymer were stained.

The slice diameter of approximately 1500 SEBS particles were determined from TEM images with a specific algorithm. It should be noticed that the three-dimensional spheres are projected on a two-dimensional plane. According to Goldsmith,[16] the following correlation between slice radius distribution $q(r)$ and sphere radius diameter $q(R)$ can be assumed for random packed particles:

$$q(r) = \frac{d}{d + 2\bar{R}}\, q(r) + \frac{2r}{d + 2\bar{R}} \times \int_r^{R_{\max}} \frac{1}{\sqrt{R^2 - r^2}}\, q(R)\, dR \quad (1)$$

Table I Polypropylenes and SEBS Used in This Study

Material		M_w[a] (g mol^{-1})	M_w/M_n	mm[b] (%)	T_m (°C)	ΔH_m[c] (%)	Block Ratio	PS–Content (%)
i-PP	VM6100H	189,600	4.6	0.96	169.7	100.3	—	—
	TM6100K	214,100	4.5	0.98	170.0	102.8	—	—
	KM6100	285,900	4.9	0.97	172.8	101.4	—	—
	JE6100	394,300	4.1	0.97	171.5	102.6	—	—
SEBS	Kraton G1652	90,000	1.04	—	—	—	1 : 5 : 1	29
	Kraton G1651	272,000	1.06	—	—	—	1 : 5 : 1	32

[a] Molecular weight from GPC versus *i*-PP standard.
[b] Triades determined by ^{13}C NMR.
[c] Melt enthalpy ΔH_m from DSC measurements with a heating rate of 10 K/min.

where d is the thickness of section and $\bar{R}$ is the average sphere radius. The first term is caused by particles in the center of the section, which are cut equatorially. The second term is caused by particles with a center out of the sectional plane. Especially with small section thicknesses d, $q(R)$ gets very sensitive on statistic errors, requiring regularization procedures. As a result of the regularization procedure according to the FTIKREG program (fast Tikhonov regularization),[17] the volume-weighted sphere radius $\bar{R}_v$ can be calculated from

$$\bar{R}_v = \frac{\int v(R) \times R \, dR}{\int v(R) \, dR} = \frac{k_R \sum_{i=1}^{n} v(R_i) \times R_i^2}{k_R \sum_{i=1}^{n} v(R_i) \times R_i} \quad (2)$$

where $v(R)$ is the volume-weighted sphere radius distribution. All dates can be numerical divided in n divisions for R and $v(R)$. The width of n is

$$k_R = \frac{\ln(R_{\max}) - \ln(R_{\min})}{n - 1} \quad (3)$$

Atomic Force Microscopy

Atomic force microscopy (AFM) experiments were performed with a Nanoscope III scanning probe microscope (Digital Instruments, Inc.). Images were obtained under ambient conditions in the tapping mode. A commercial Si cantilever with force constants of 13–70 N/m was used. Height, amplitude, and phase images were recorded simultaneously. Images were taken at the fundamental resonance frequency of the Si cantilever and recorded with typical scan speed of 0.3–1 line/s using scan heads with a maximum range of 16 × 16 μm. The free resonance amplitude was 45 nm, and the set point amplitude was about 30 nm. The sample preparation corresponds to that described for TEM. Instead of sections for TEM sectioned surfaces were used for AFM.

RESULTS AND DISCUSSION

Characterization of the Blend Components

Melt viscosities and mechanical properties of *i*-PP and SEBS were determined as a function of molecular weight. The results are listed in Table II.

Figure 1 shows the dynamic viscosity η' of *i*-PP in dependence on frequency, determined by rheological experiments according to Eckstein et al.[18] In the whole range of frequency, the dynamic viscosity increases with increasing molecular weight.

The influence of *i*-PP molecular weight on zero shear viscosity η_0, defined as dynamic viscosity at very low frequencies, and melt flow index (MFR) is depicted in Figure 2. As already seen in Figure 1, η_0 increases with increasing *i*-PP molecular weight, and melt flow index simultaneously decreases. As a consequence of enhanced melt viscosity, the specific energy of the extrusion process $E_{\text{spec.}}$ increases, as seen in Table II. With increasing molecular weight Young's modulus, yield stress and notched Izod impact strength of *i*-PP, determined by tensile and impact tests, increase, and elongation to break decreases, as discussed in the next section.

The melt viscosity of SEBS also increases with increasing molecular weight, but it is not possible to measure zero shear viscosity and MFR of high-molecular SEBS (Kraton G1651) because this material is too viscous for rheological and melt flow experiments at 200°C. As expected, stiffness of

Table II Physical and Mechanical Properties of Polypropylenes and SEBS

Material	M_w[a] (g mol^{-1})	η_0[b] (Pas)	MFR[d] (g (10 min)$^{-1}$)	E_{spec}[e] (kWh kg^{-1})	Young's Modulus (MPa)	Yield Stress (MPa)	Elongation to Break (%)	Notched Izod Impact Strength (kJ m^{-2})
i-PP	189,600	2,600	20.5	0.21	1.036	26.3	>500	2.1
	214,100	7,700	14.1	0.22	1.356	27.3	>500	2.2
	285,900	40,600	3.5	0.26	1.492	29.8	103	2.8
	394,300	66,200	2.3	0.27	1.548	30.8	79	3.1
SEBS	90,000	130,400	1.3	—	22	—	>500	dnb[f]
	272,000	—[c]	—[c]	—	13	—	>500	dnb[f]

[a] Molecular weight from GPC versus *i*-PP standard.
[b] Zero shear viscosity η_0 from dynamic experiments at 200°C.
[c] Melt viscosity too high for measurements.
[d] Melt flow index (MFR) at 230°C with 2.16 kg.
[e] Specific energy for extrudation.
[f] Did not break.

SEBS is very low, and impact strength and elongation to break are very high.

Mechanical Properties of *i*-PP–SEBS Blends

Mechanical properties of *i*-PP and *i*-PP–SEBS blends were determined as a function of *i*-PP and SEBS molecular weight and composition. The results are listed in Table III.

In the investigated molecular weight interval of M_w = 190,000 to 400,000 g/mol, Young's modulus of *i*-PP is doubled by doubling *i*-PP molecular weight. This dependency is pronounced at lower molecular weights and only marginal above 250,000 g mol^{-1}, as seen in Figure 3. Also, tensile yield stress increases with increasing *i*-PP molecular weight (Fig. 4). These effects are caused by enhanced entanglements due to longer polymer chains. It is well known that SEBS as an elastomeric phase reduces stiffness and tensile yield

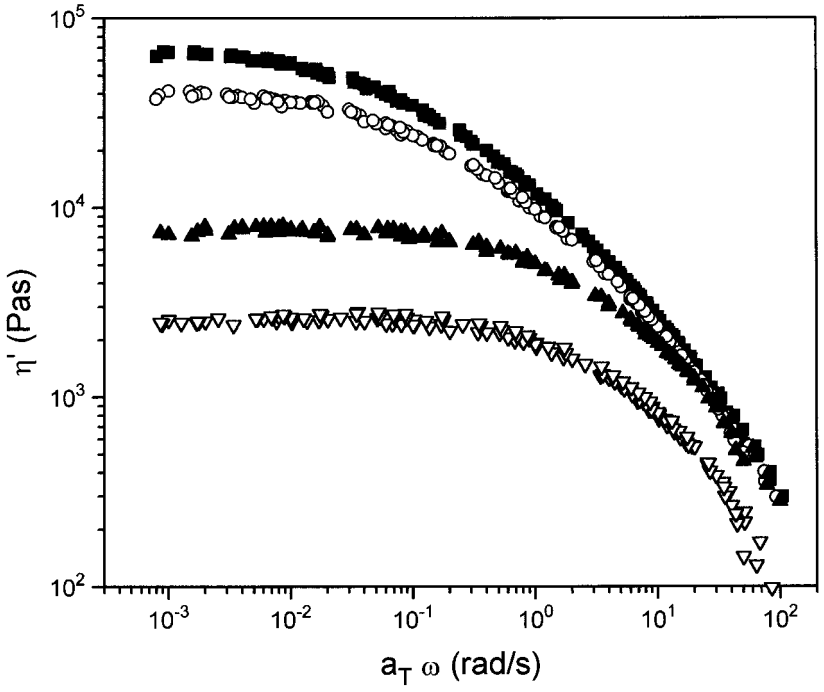

Figure 1 Dynamic viscosity η' of *i*-PP with different molecular weights versus reduced angular frequency ωa_T at the reference temperature T_0 = 200°C: (■) M_w = 394,300, (○) 285,900, (▲) 214,100, and (▽) 189,600 g mol^{-1}.

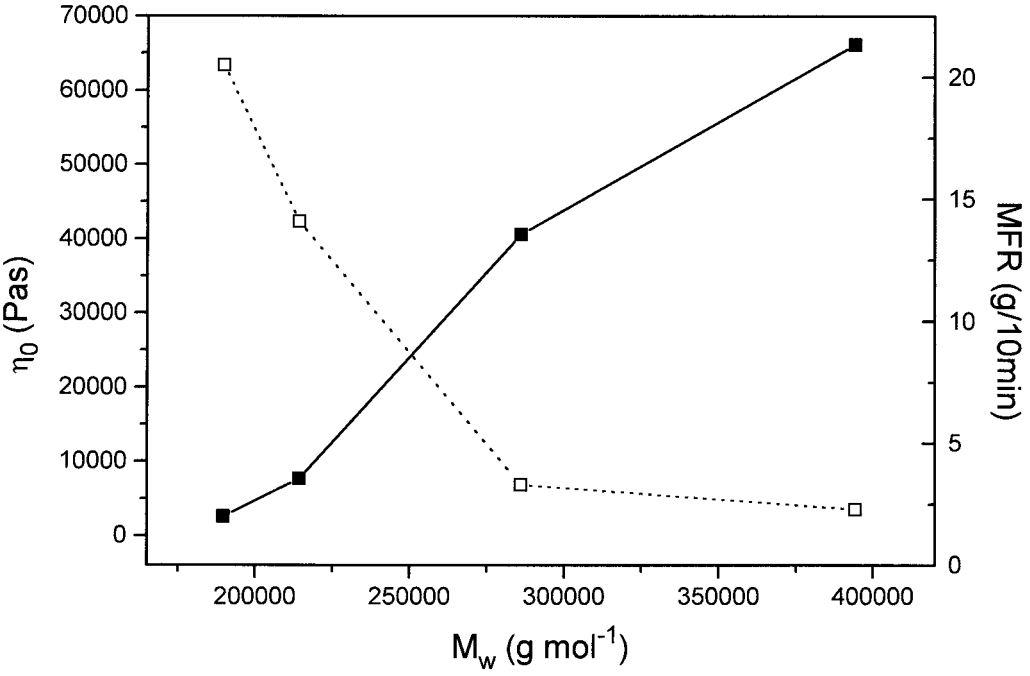

Figure 2 (■) Zero shear viscosity η_0 and (□) melt flow index (MFR) as a function of *i*-PP molecular weight.

stress.[5,6] As a consequence, the corresponding values of *i*-PP blends are lower than those of pure *i*-PP, but the influence of molecular weight is identical to that of pure *i*-PP. It is obvious from the figures that the dependency of Young's modulus and tensile yield stress of *i*-PP–SEBS blends on *i*-PP molecular weight is dependent primarily on the properties of *i*-PP matrix. Morphology, for ex-

Table III Particle Size *d*, Interparticulare Distance *A*, and Mechanical Properties of *i*-PP–SEBS Blends

i-PP M_w (g mol^{-1})	SEBS M_w (g mol^{-1})	(Vol %)	λ_0[a]	Young's Modulus (MPa)	Yield Stress (MPa)	Notched Izod Impact Strength (kJ m^{-2})	*d* (μm)	*A* (μm)
189.600	90.000	10	50.2	953	23.5	3.6	0.45	0.33
		15	50.2	855	21.9	6.5	0.55	0.28
		20	50.2	813	20.1	29.6	0.49	0.19
	270.000	10	—	843	20.9	4.5	0.76	0.56
		15	—	791	18.9	6.6	0.72	0.37
		20	—	691	17.5	27.8	0.69	0.26
214.100	90.000	15	16.9	1.043	23.2	4.6	0.50	0.27
	270.000	15	—	958	20.1	7.4	0.65	0.34
285.900	90.000	10	3.21	1.170	26.7	13.4	0.19	0.14
		15	3.21	1.154	25.0	25.1	0.29	0.15
		20	3.21	998	23.0	33.7	0.21	0.08
	270.000	10	—	1.146	24.8	8.1	0.59	0.43
		15	—	1.095	22.8	27.4	0.46	0.24
		20	—	902	20.3	38.4	0.55	0.21
394.300	90.000	15	1.97	1.175	25.3	25.4	0.26	0.13
	270.000	15	—	1.124	23.2	28.5	0.34	0.18

[a] Zero shear viscosity ratio $\lambda_0 = \eta_{0,d}/\eta_{0,m}$.

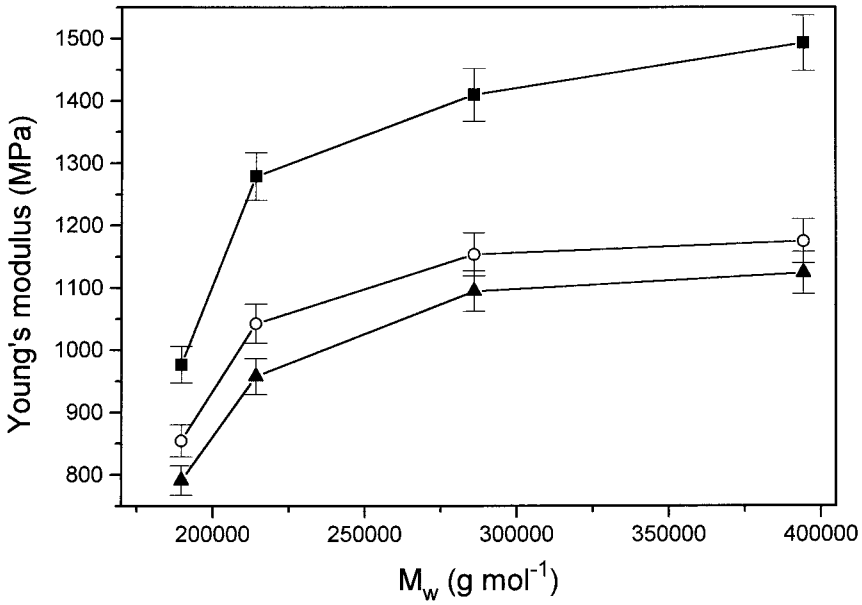

Figure 3 Young's Modulus versus *i*-PP molecular weight M_w: (■) *i*-PP, (○) *i*-PP with 15 vol % SEBS (Kraton G1652), and (▲) *i*-PP with 15 vol % SEBS (Kraton G1651).

ample, SEBS particle size, does not effect neither Young's modulus nor yield stress.

Figure 4 shows that blends with lower molecular weight SEBS have higher yield stresses than blends with higher molecular weight SEBS. Previous work has shown, that at the *i*-PP–SEBS interface, interdiffusion occurs, improving interfacial interactions.[19] Assuming that interdiffusion is favored for lower molecular weight of SEBS, adhesion and, consequently, tensile yield stress of corresponding *i*-PP blends is improved in comparison to blends with higher molecular weight SEBS. As seen in Figure 5, notched Izod impact strength of *i*-PP marginally increases with increasing *i*-PP molecular weight. Blends with 15 vol % SEBS have a sharp brittle–tough transition between *i*-PP molecular weight of 214,100 and 285,900 g mol^{-1}. In other words, in *i*-PP with mo-

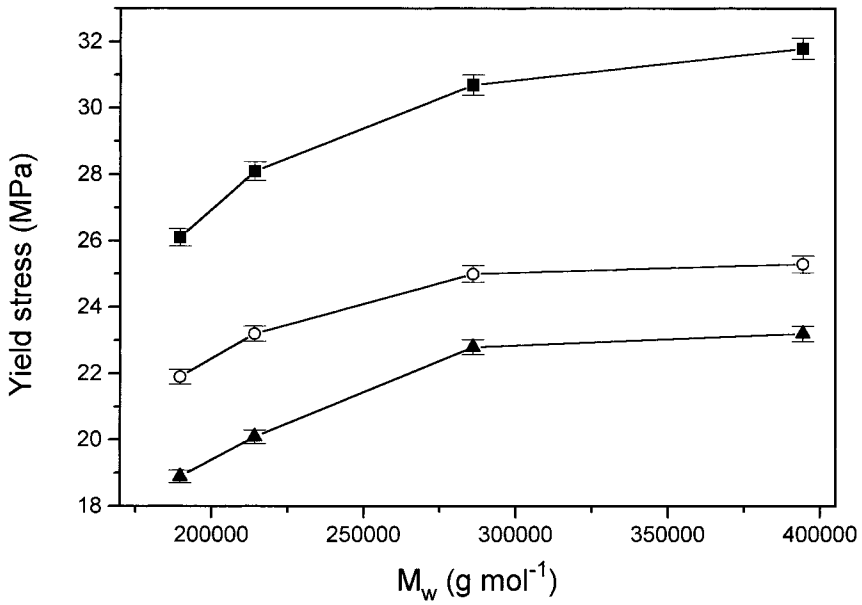

Figure 4 Yield stress versus *i*-PP molecular weight M_w: (■) *i*-PP, (○) *i*-PP with 15 vol % SEBS (Kraton G1652), and (▲) *i*-PP with 15 vol % SEBS (Kraton G1651).

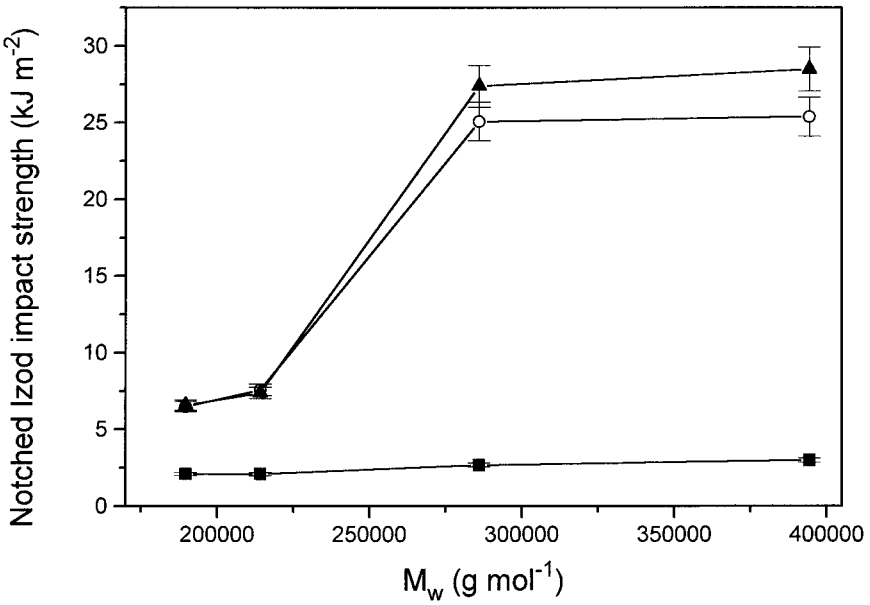

Figure 5 Notched Izod impact strength versus *i*-PP molecular weight M_w: (■) *i*-PP, (○) *i*-PP with 15 vol % SEBS (Kraton G1652), (▲) and *i*-PP with 15 vol % SEBS (Kraton G1651).

lecular weight higher than 250,000 g mol^{-1}, 15 vol % SEBS are sufficient to achieve ductile behavior; in *i*-PP with molecular weight lower than 250,000 g mol^{-1}, at least 20 vol % SEBS are necessary (also see Table III).

In contrast to Young's modulus and tensile yield stress, this sharp brittle–tough transition cannot be explained only by the influence of *i*-PP molecular weight itself. Morphological aspects, such as SEBS particle size and matrix ligament thickness, should be responsible for this effect and are investigated in the next sections.

Determination of SEBS Particle Size

Figure 6 shows TEM images of ultrathin sections of *i*-PP (KM6100) blended with 10 vol % SEBS (Kraton G1652). The dark areas in the TEM images are polystyrene domains of SEBS after 3-min staining with RuO_4. At low magnifications, the whole SEBS particles are dark; at higher magnifications, the microphase separation of SEBS can be seen.

Another method to determine SEBS particle size is AFM. It is known that AFM phase imaging offers good material contrast.[20] Figure 7 shows AFM phase images in tapping mode of sectioned surface of *i*-PP (KM6100) blends with 10 vol % SEBS (Kraton G1652). Particle size and particle size distribution corresponds to that obtained by TEM. Because of surface destruction during sectioning, the triblock copolymer morphology is only difficult to see.

The SEBS particle diameter of *i*-PP–SEBS blends, determined as described above, are listed in Table III. The particle size is strongly dependent on zero shear viscosity of *i*-PP and SEBS and thus on *i*-PP and SEBS molecular weight, as clearly seen in Figure 8. With increasing *i*-PP zero shear viscosity η_0 and molecular weight, respectively, SEBS particle size decreases. The SEBS particles in blends with high-molecular-weight SEBS are always larger than those of blends with low-molecular-weight SEBS. The dotted lines are obtained by an exponential fitting procedure.

Under assumption of Newtonian behavior, the influence of rheological properties, for example, the melt viscosity ratio, and interfacial interactions can be expressed by two dimensional parameters, the viscosity ratio λ and the capillary number κ,[21,22] as follows:

$$\lambda = \frac{\eta_d}{\eta_m} \tag{4}$$

$$\kappa = \frac{\eta_m \dot{\gamma} R}{\nu} \tag{5}$$

where η_m is the melt viscosity of the *i*-PP matrix and η_d is that of the dispersed SEBS, $\dot{\gamma}\eta_m$ is the local shear stress, R is the particle radius, and ν is the interfacial tension. For good dispersion, a

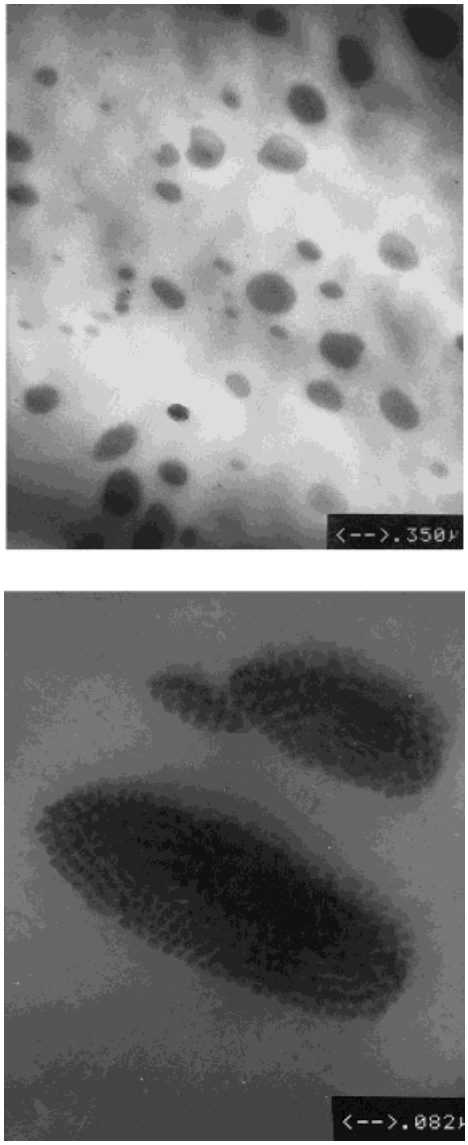

Figure 6 TEM images of *i*-PP (KM6100) blends with 10 vol % SEBS (Kraton G1652) after 3 min of staining with RuO_4.

low viscosity ratio λ and a high capillary number κ are required, as achieved for a high molecular weight of the *i*-PP matrix and a low molecular weight of dispersed SEBS, although a minimum molecular weight of dispersed SEBS phase is required in order to enable entanglements. It was not possible to determine the actual local shear stress $\dot{\gamma}\eta_m$ in the different processing zones of the extruder. Consequently, the melt viscosities η_m and η_d of *i*-PP and SEBS, which are dependent on frequency, are unknown. As already seen in Figure 1, melt viscosity of *i*-PP increases with increasing molecular weight in the whole range of frequency, so the viscosity ratio λ can be replaced by the zero shear viscosity ratio λ_0, following the same conditions for good dispersion as λ. Table III shows that λ_0 has to be smaller than 3.2 to achieve ductile blends. Even if the capillary number can't be quantitatively calculated because $\gamma\eta_m$ is unknown, a tendency can be derived. The interfacial tensions are constant because the variation of *i*-PP and SEBS molecular weight does not strongly affect interfacial tension. Consequently, melt viscosities of *i*-PP and SEBS are the decisive factors for SEBS particle size of the *i*-PP–SEBS blends. As seen in Table III, SEBS particle diameter is independent of the SEBS volume fraction, indicating a low tendency for coalescence.

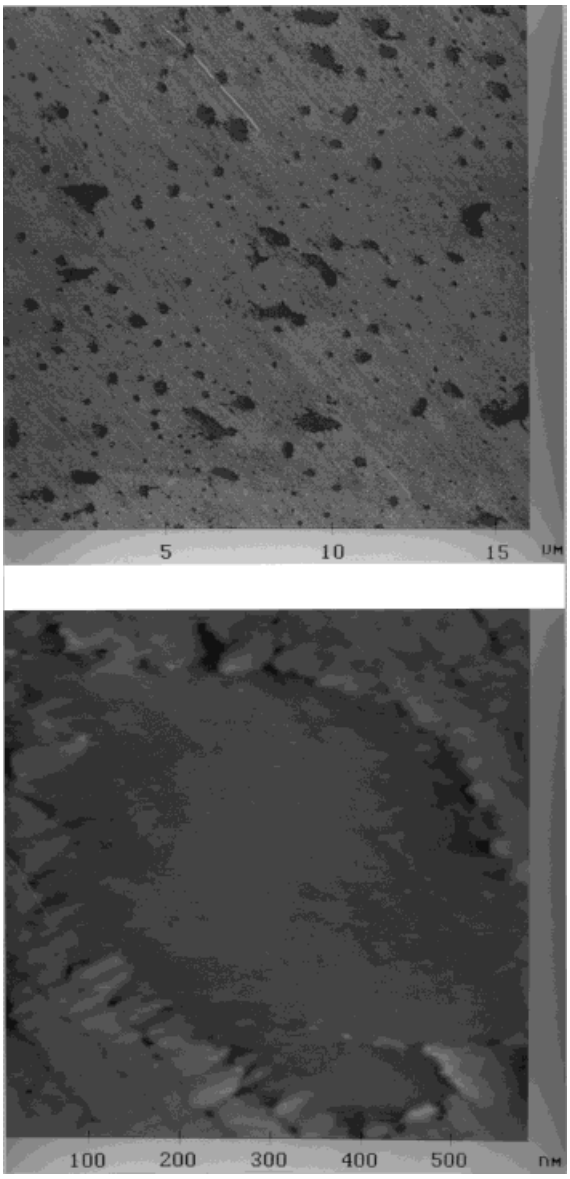

Figure 7 AFM phase images on sectioned surfaces of *i*-PP (KM6100) blends with 10 vol % SEBS (Kraton G1652).

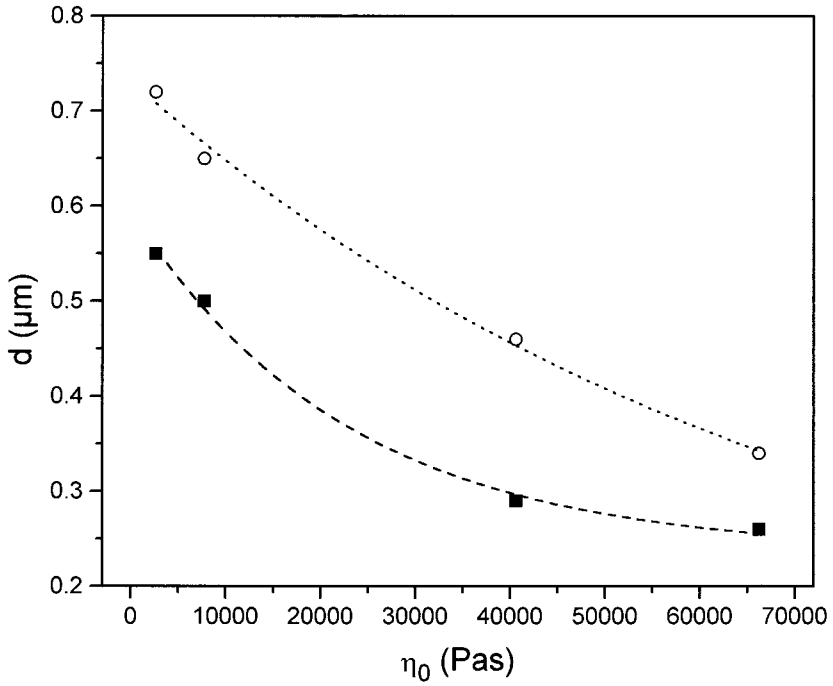

Figure 8 Particle diameter d as a function of zero shear viscosity η_0: (■) i-PP with 15 vol % SEBS (Kraton G1652) and (○) i-PP with 15 vol % SEBS (Kraton G1651). Dotted lines represent determination by exponential fitting.

Influence of Particle Size on Mechanical Properties

As already mentioned, Young's modulus and tensile yield stress of i-PP–SEBS blends are independent of SEBS particle size. In Figure 7, the notched Izod impact strength of i-PP blends is plotted against SEBS particle diameter d with varying SEBS volume fraction. With 10 vol % SEBS, impact strength only marginally increases when the particle sizes are smaller than 0.4 μm. Blends with 15 vol % have a sharp brittle–tough transition at about 0.5 μm. Smaller particle sizes, determined for blends based on i-PP with higher molecular weight, cause tough behavior, and bigger particles cause brittle behavior. All investigated blends with 20 vol % are tough, even at particle diameters of about 0.7 μm. At this volume fraction, the formation of a SEBS network cannot be excluded, although TEM images did not reveal such structures. It is obvious from Figure 9 that critical particle diameter for brittle–tough transition is strongly dependent on the SEBS volume fraction.

The critical matrix ligament thickness and critical interparticle distance, respectively, for the brittle–tough transition is independent on elastomer volume fraction and, thus, a material constant. In accordance to Wu's percolation model,[10] interparticle distance A can be correlated with average particle size d, as follows:

$$A = d \times \left(\sqrt[3]{\frac{\pi}{6\varphi_e}} - 1 \right) \qquad (6)$$

The interparticle distance A of i-PP/SEBS blends is listed in Table III. With increasing i-PP molecular weight and zero shear viscosity, respectively, and increasing SEBS volume fraction, interparticle distance decreases. On the other hand, interparticle distance decreases with SEBS molecular weight and zero shear viscosity ratio λ', respectively.

The influence of interparticle distance on notched Izod impact strength is depicted in Figure 10. In accordance with the results of Wu for nylon–rubber blends, a critical value can be determined, which is independent of the elastomer volume fraction. The brittle–tough transition of i-PP blends occurs at about 0.27 μm. If the matrix ligament is thinner than this value, effective shear yielding can be assumed, improving impact strength significantly.[12,13] This critical matrix ligament thickness is similar to results from Wu,

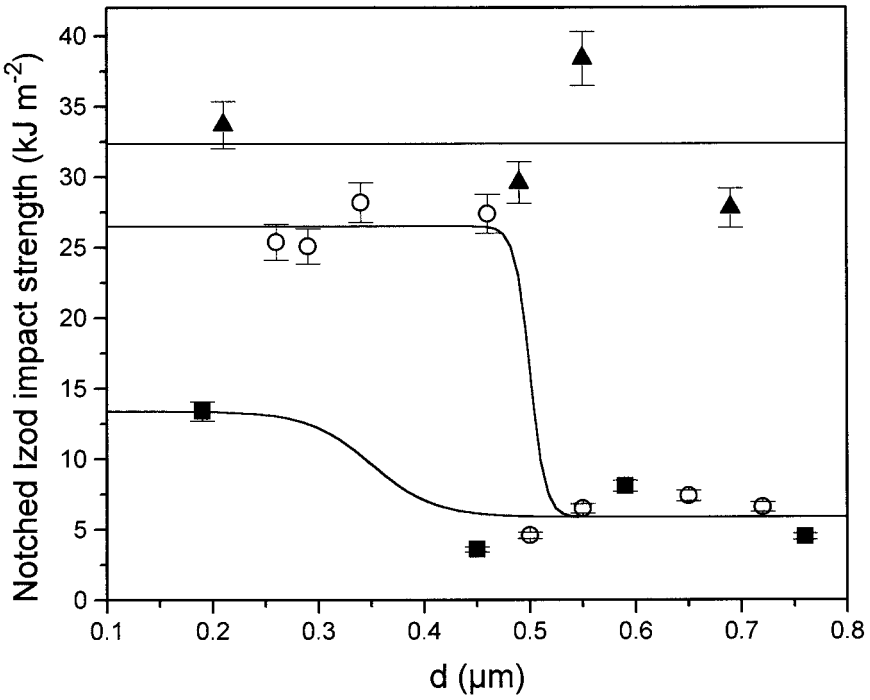

Figure 9 Notched Izod impact strength as a function of particle diameter d: (■) *i*-PP with 10 vol % SEBS, (○) *i*-PP with 15 vol % SEBS, and (▲) *i*-PP with 20 vol % SEBS.

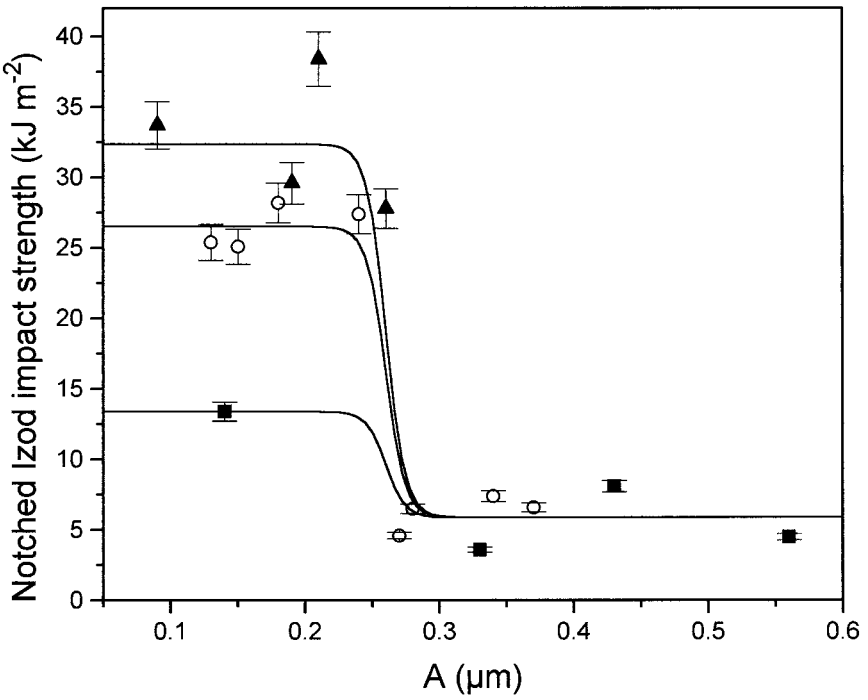

Figure 10 Notched Izod impact strength as a function of interparticle distance A: (■) *i*-PP with 10 vol % SEBS, (○) *i*-PP with 15 vol % SEBS, and (▲) *i*-PP with 20 vol % SEBS.

who found for nylon–rubber blends a value of 0.30 μm.[10,11]

The authors thank Shell Research in Louvain-la-Neuve, Belgium, for supporting this study.

REFERENCES

1. E. Martuscelli, in *Polypropylene: Structure, Blends and Composites,* Vol. 2, J. Karger-Kocsis, Ed., Chapman and Hall, London, 1995, p. 95.
2. E. P. Moore, in *Polypropylene Handbook,* Hanser Verlag, München, 1996.
3. C. R. Lindsey, D. R. Paul, and J. W. Barlow, *J. Appl. Polym. Sci.,* **1,** 26 (1981).
4. C. R. Dreyfuss, L. J. Fetters, and D. R. Hansen, *Rubber Chem. Technol.,* **53,** 728 (1980).
5. A. K. Gupta and S. N. Purwar, *J. Appl. Polym. Sci.,* **31,** 535 (1986).
6. A. K. Gupta and S. N. Purwar, *J. Appl. Polym. Sci.,* **29,** 3513 (1984).
7. A. K. Gupta and S. N. Purwar, *J. Appl. Polym. Sci.,* **29,** 1079 (1984).
8. A. K. Gupta and S. N. Purwar, *J. Appl. Polym. Sci.,* **29,** 1595 (1984).
9. A. Margolina and S. Wu, *Polymer,* **29,** 2170 (1988).
10. S. Wu, *Polymer,* **26,** 1855 (1985).
11. S. Wu, *J. Appl. Polym. Sci.,* **35,** 549 (1988).
12. R. J. M. Borggreve, R. J. Gaymans, J. Schuijer, and F. I. Housz, *Polymer,* **28,** 1489 (1987).
13. R. J. M. Borggreve and R. J. Gaymans, *Polymer,* **29,** 1441 (1988).
14. M. C. M. Van der Sanden, H. E. H. Meijer, and P. J. Lemstra, *Polymer,* **34,** 2148 (1993).
15. L. C. Sawyer and D. T. Grubb, *Polymer Microscopy,* Chapman & Hall, London, 1982.
16. P. J. Goldsmith, *J. Brit. J. Appl. Phys.,* **18,** 813 (1967).
17. J. Weese, *Comput. Phys. Commun.,* **69,** 99 (1992).
18. A. Eckstein, C. Friedrich, A. Lobbrecht, R. Spitz, and R. Mülhaupt, *Acta Rheo.,* **48,** 41 (1997).
19. S. Setz, F. Stricker, J. Kressler, T. Duschek, and R. Mülhaupt, *J. Appl. Polym. Sci.,* **59,** 1117 (1996).
20. G. Bar, Y. Thomann, R. Brandsch, and H.-J. Cantow, *Langmuir,* **13,** 3807 (1997).
21. L. A. Utracki and Z. H. Shi, *Polym. Eng. Sci.,* **32,** 1824 (1992).
22. L. A. Utracki, *Two-Phase Polymer Systems,* Hanser-Verlag, München, 1991.